

# A quantitative assessment of ontogeny and molting in a Cambrian radiodont and the evolution of arthropod development

## Article

**Cite this article:** Moysiuk J, Caron J-B (2024). A quantitative assessment of ontogeny and molting in a Cambrian radiodont and the evolution of arthropod development. *Paleobiology* 50, 54–69. <https://doi.org/10.1017/pab.2023.18>

Received: 8 November 2022  
Accepted: 18 May 2023

**Corresponding author:**  
Joseph Moysiuk;  
Email: [joe.moysiuk@mail.utoronto.ca](mailto:joe.moysiuk@mail.utoronto.ca)

Joseph Moysiuk<sup>1</sup>  and Jean-Bernard Caron<sup>1,2</sup> 

<sup>1</sup>Department of Ecology and Evolutionary Biology, University of Toronto, 25 Willcocks Street, Toronto, Ontario M5S 3B2, Canada; and Department of Natural History, Royal Ontario Museum, 100 Queen's Park, Toronto, Ontario M5S 2C6, Canada

<sup>2</sup>Department of Earth Sciences, University of Toronto, 22 Ursula Franklin Street, Toronto, Ontario, M5S 3B1, Canada

### Non-technical Summary

Radiodonta is a group of early arthropods, distantly related to living insects and spiders, that provides insight into the origin of the segmented body plan shared by these animals. Radiodonts include some of the largest animals from the Cambrian Period; however, little has been known about their development due to a lack of juvenile specimens. We present an analysis of development of the radiodont *Stanleycaris* based on 265 exceptionally well-preserved specimens from the Cambrian Burgess Shale, ranging in size from 10 to 83 mm. We show that several aspects of the body shape of *Stanleycaris* changed as it grew. For example, the eyes were relatively larger in the smallest individuals, suggesting that juveniles were advanced visual predators. Additionally, segments were added sequentially at the rear of the body, a common developmental trait among arthropods. In light of the early evolutionary divergence of radiodonts from other arthropods, this finding provides direct evidence for a deep origin of this developmental mode. Finally, using a newly devised approach, we find evidence for two distinct fossil types of *Stanleycaris*, representing carcasses and molted exoskeletal remains, respectively. Based on comparison with fossils of other species, the general pattern of molting in *Stanleycaris* is likely shared among radiodont species and potentially other early arthropods. Altogether, our study demonstrates the first detailed view of the early development of a radiodont, providing key new evidence about the evolution of development at the origin of the arthropod body plan.

### Abstract

Radiodonta is a clade of stem euarthropods of central importance to our understanding of the evolution of this phylum. Radiodonts include some of the largest early Paleozoic animals; however, little is known about their ontogeny. We present an analysis of molting patterns and ontogeny in the radiodont *Stanleycaris* based on 265 exceptionally preserved specimens from the mid-Cambrian (Wuliuan) Burgess Shale. Ranging in size from 10 to 83 mm, they constitute the most extensive radiodont ontogenetic series known. Using a novel morphospace approach, we show that putative carcasses and exuviae can be quantitatively distinguished by the particular suites of structures preserved and their modes of preservation. We propose that *Stanleycaris*, and probably other radiodonts, molted via a suture near the anterior of the trunk. Similar anterior molting strategies, with a suture located at the head–trunk boundary, are shared with some Cambrian euarthropods and are potentially ancestral. Allometric analyses suggest that as *Stanleycaris* body size increased, the head sclerite and neck became relatively broader, while the trunk and flaps became slightly longer. The eyes developed precociously, indicating an important role of visual processing in juveniles. Finally, we find evidence for an initial anamorphic developmental phase, where segment number increased at least from 11 or 12 up to 17, followed by an epimorphic phase, in which growth continued without segment addition. This is consistent with the hypothesis that finite postembryonic segment addition (hemianamorphosis) is ancestral for arthropods and refines the timing of the origin of this important developmental mode.

### Introduction

Integrating insights from evolutionary developmental biology and paleontology has immensely enriched our understanding of the origins of animal body plans. Reconstructing and analyzing ontogeny in the fossil record has thus become a major research agenda (Raff 2007). To this end, Arthropoda is an ideally suited group, considering its high diversity and disparity and excellent fossil record since the Cambrian Period. For the same reasons, the study of arthropods has also been important historically in considerations of the Cambrian explosion (Gould 1989; Daley et al. 2018; Chipman and Edgecombe 2019; Aria 2020). Ongoing

© The Author(s), 2023. Published by Cambridge University Press on behalf of The Paleontological Society. This is an Open Access article, distributed under the terms of the Creative Commons Attribution-NonCommercial-NoDerivatives licence (<http://creativecommons.org/licenses/by-nc-nd/4.0>), which permits non-commercial re-use, distribution, and reproduction in any medium, provided that no alterations are made and the original article is properly cited. The written permission of Cambridge University Press must be obtained prior to any commercial use and/or adaptation of the article.

**PALEOBIOLOGY**  
A PUBLICATION OF THE  
 PALEONTOLOGICAL SOCIETY

 **CAMBRIDGE**  
UNIVERSITY PRESS



discoveries continue to push the boundaries of our knowledge of the ontogeny of early-diverging groups, collectively informing the origin and diversification of the arthropod body plan.

Ontogenetic series of varying completeness have been described for a range of early arthropods. The greatest volume of work concentrates on trilobites, whose calcified terga are well preserved from all postembryonic life stages across numerous taxa (reviewed in Hughes 2007; Hopkins 2017; Hughes et al. 2021). The development of soft tissue structures in trilobites remains virtually unknown (but see Eriksson and Terfelt 2012). Another rich source of ontogenetic data comes from specimens preserved via high-fidelity Orsten-type phosphatization, representing larval stages of primarily total group mandibulates (Haug et al. 2014; Eriksson and Waloszek 2016). The adult representatives of these taxa often remain obscure, although a few connections with Burgess Shale-type macrofossils have been proposed (Aria et al. 2015; Aria and Caron 2017; Moysiuk and Caron 2019a). In addition, Burgess Shale-type deposits have yielded rare examples of juvenile arthropods alongside adults of the same species, enabling conclusions about segment addition and allometry (García-Bellido and Collins 2006; Zhang et al. 2007; Haug et al. 2011; Fu et al. 2014, 2018; Aria et al. 2015; Liu et al. 2016; Mayers et al. 2018; Izquierdo-López and Caron 2021; Yang et al. 2021; Liu et al. 2022). Finally, related evidence for how fossil arthropods underwent growth comes from the preserved record of ecdysis (Daley and Drage 2016). While these records of Cambrian arthropod ontogenies have yielded spectacular insights, the development of many groups remains poorly known.

Radiodonta is perhaps the only major extinct clade whose phylogenetic position in the euarthropod stem group is nearly uncontroversial, and understanding development in this group has great importance for reconstructing ancestral states for the phylum (Edgecombe 2020). Until now, developmental data for radiodonts have been scarce. Liu et al. (2018) documented a single ca. 2 cm specimen of *Lyrarapax*, showing that an adult-like morphology had already developed by this juvenile stage. Paterson et al. (2020) demonstrated probable ontogenetic increases in ommatidial size and marginal addition of new ommatidia in *Anomalocaris* aff. *canadensis* and '*Anomalocaris*' *briggsi*. Caron and Moysiuk (2021) found evidence for allometric changes in carapace shape in *Cambroraster falcatus*. Limited sample sizes, the rarity of complete specimens, and the near absence of small juvenile individuals across all species have necessarily constrained these attempts at reconstructing radiodont ontogeny. Here, we begin to fill this gap with an analysis of the Burgess Shale radiodont *Stanleycaris*, based on a large collection of fossil material curated at the Royal Ontario Museum (Moysiuk and Caron 2022). First, using a novel "taphomorphospace" approach to understand taphonomic variations in specimen morphology, we are able to distinguish between exuviae and carcasses, shedding light on radiodont ecdysis. Second, we examine patterns of allometry and segment addition using standard morphometric methods. Taken together, our results provide the most complete picture yet available of radiodont ontogeny.

## Material and Methods

### Fossil Material

A collection of 265 specimens of *Stanleycaris* is available from the Wuliuan Burgess Shale Formation (Supplementary Fig. 1). The best-preserved material, representing the majority of examined

specimens (243), come from the Collins Quarry (Emerald Lake Oncolite Member) on "Fossil Ridge" in Yoho National Park. This material was collected by the Royal Ontario Museum over the course of several seasons (1984–1993), from two sublocalities: "Ehmaniella Zone" (EZ) and "Upper Ehmaniella" (UE) (Fletcher and Collins 1998; Caron 2005). Additional small collections (15) come from lower sections on "Fossil Ridge" (Raymond and Walcott Quarries), as well as Odaray Mountain. Rare (7) specimens of *Stanleycaris* sp. also occur in the older *Glossopleura* Zone on Mount Stephen and Mount Field. See Moysiuk and Caron (2022) for a description of this material and relevant anatomical terms.

Other collections of mostly disarticulated *Stanleycaris* material come from Stanley Glacier and other Stephen Formation outcrops in Kootenay National Park. These were described elsewhere (Caron et al. 2010; Moysiuk and Caron 2021; see also Supplementary Discussion and Supplementary Fig. 2). Three representative specimens were included in this study for comparison.

### Taphomorphospace

Two qualitatively different modes of preservation can be seen in body fossils of *Stanleycaris* (Moysiuk and Caron 2022). We hypothesized that these may represent carcasses and exuviae; however, the quantitative distinctiveness of these taphomorphs has not yet been demonstrated. It remains possible that the two putatively distinct fossil groups in fact represent end-members of a more continuous morphological series, arising, for example, through stepwise decay of characters. Here we evaluate these scenarios using a novel taphonomic morphospace ("taphomorphospace") approach with our large sample of *Stanleycaris* specimens.

The term "taphomorphospace" was previously coined to refer to a morphospace of fossil specimens incorporating some component of taphonomic variation (Hedrick and Dodson 2013), a definition equally applicable here. The main distinction of our approach is that we intentionally consider morphologies that we think are likely to vary due to taphonomic factors because this variation may be biologically meaningful. The logic is as follows. The preservation—or lack thereof—of different structures or tissue types can be informative about differing taphonomic histories (e.g., Saleh et al. 2020). We therefore anticipate predictable differences in the taphonomy—and resulting specimen morphology—of carcasses and exuviae owing to their differing composition and history (Daley and Drage 2016). If our collection includes distinct carcass and molt taphomorphs, we hypothesize that cluster analysis will support a clear grouping structure in taphomorphospace, with an association between specific morphological variables (e.g., internal organs, structures separated during molting) and intergroup variation. By contrast, if specimens belong to a more or less continuous decay series characterized by stepwise loss of structures, there should be no obvious grouping structure in taphomorphospace. Instead, hierarchical clustering should yield a pectinate tree with short branches separating any clusters, and progression along the tree backbone should be associated with the gradient of character loss (Supplementary Fig. 3). Naturally, these contrasting scenarios are idealizations, and some combination of these patterns might be expected in real data.

To produce the taphomorphospace, we made use of the comprehensive collection of 265 specimens (Supplementary Data 1.2). We excluded 45 specimens for which a large part of the body was lost due to breakage of the slab to avoid introducing dissimilarity

artifacts caused by missing data (Lloyd 2016). For the remaining 223 specimens, we coded a series of binary presence–absence variables based on whether or not a structure was visible. A structure was coded as present if any part of it was visible. For detailed explanation of anatomies and terminology, see Moysiuk and Caron (2022). For the purposes of this observation matrix, the variable “Trunk” refers only to the axial trunk cuticle, as the flaps, gills, and internal organs are coded as independent variables. An additional binary variable coded for the presence of obvious disarticulation of any body parts, that is, when parts that should be anatomically connected were preserved separated, but in close association. Cases where body parts were entirely missing did not qualify as disarticulation, as these could simply be hidden or not preserved.

Statistical analyses were carried out in R v. 4.1.3 (R Core Team 2020) using the packages cluster 2.1.2 (Maechler et al. 2019), vegan 2.5-7 (Oksanen et al. 2020), ade4 1.7-19 (Dray and Dufour 2007), shipunov 1.17 (Shipunov et al. 2022), dendextend 1.15.2 (Galili 2015), vcd 1.4-9 (Meyer et al. 2007), and vcdExtra 0.8-0 (Friendly 2022). All code is available in Supplementary Data 1.1.

From our data matrix, we calculated distance matrices. The joint absence of structures might be informative, as both could have been lost through the same process (e.g., decay or removal during ecdysis), which would favor the use of simple matching distances. On the other hand, it is possible that structures not visible in a particular specimen could be covered by matrix or other body parts rather than truly absent. This could make the case for preference of Jaccard distances, which consider only joint presences to be informative. We therefore performed analyses with both distance metrics and compared their respective results.

We conducted principal coordinates analysis (PCoA), k-means clustering, and unweighted pair group method with arithmetic mean hierarchical clustering (UPGMA; selected as the best method by the function *PlotBest.hclust*) on the distance matrices. Silhouette plots were employed to detect possible incorrect group assignments. Groups identified by hierarchical clustering were mapped into the PCoA. For the PCoA, the magnitude of negative eigenvalues was small, so no correction was performed. Percentages of variation represented on each PCo axis were calculated considering only the subset of positive eigenvalues (Hopkins 2016). We determined the number of significant axes using scree plots and the broken stick model (Jackson 1993). The association of Burgess Shale locality with variation in taphomorphospace was tested with permutational multivariate analysis of variance (PERMANOVA). We also used chi-square tests with simulated *p*-values ( $1 \times 10^6$  replicates) to evaluate the association of locality with cluster assignment, excluding any specimens for which assignment was ambiguous. To estimate the association between the original binary variables and the PCo axes, analogous to loadings in principal component analysis, we used Goodman and Kruskal's gamma statistic, following the approach of Foote (1995). This statistic ranges from  $-1$  to  $1$  indicating perfect negative or positive association, respectively. Each axis was divided into four equal intervals, from which contingency tables were tabulated and the gamma statistic computed. We then plotted the gamma statistics for variables significantly (95% confidence interval not overlapping 0) associated with one or both axes as vectors for each PCoA biplot. The relative lengths of these vectors were calculated to be proportional to their gamma statistics.

## Morphometrics

A series of linear measurements representing aspects of the morphology of *Stanleycaris* (Supplementary Fig. 4) were taken by measuring carcass specimens in the freeware ImageJ (Schneider et al. 2012). Specimens buried at oblique angles or showing evidence of partial overfolding or fragmentation were excluded, leaving a total of 56 specimens. Most of these specimens came from the Collins Quarry, though a large specimen from the West Stephen locality was also sufficiently complete to be included. This restricted subset of data, used in all morphometric analyses, is included in a separate file for convenient processing (Supplementary Data 1.3). Where certain measurements could not be taken because the specimen was incomplete, these were omitted from biplots containing the missing measures, so that actual sample size for each measure was lower—these are indicated in each biplot. To assess allometry, we selected total body length as a size metric. Measurement of this variable excluded the terminal filiform blades, as these are often unclear in the fossils. Each value for the other measures was then divided by size and transformed by taking the natural logarithm, creating a series of shape variables. Specimens vary in burial orientation, with the majority being flattened either dorsoventrally or oblique-laterally. As a consequence, some measurements (e.g., total body length, neuropil diameter) could be taken for nearly all specimens, while others could only be taken for the subset preserved in a particular orientation (e.g., trunk width).

We generated kernel density curves for the frequencies of each standardized shape variable and tested for deviation from normality using Shapiro-Wilk tests. Allometry was investigated by regressing shape variables on size. Using functions in the package *lmodel2* 1.7-3 (Legendre 2018), we calculated both ordinary least squares (OLS) and standard major axis (SMA) regression models for each shape–size comparison (Kilmer and Rodríguez 2017). Significance of the OLS model was calculated using permutation tests (Legendre 2018) with 1000 permutations each.

Some trilobites exhibit a change in allometry corresponding to the transition between anamorphic and epimorphic developmental phases (Holmes et al. 2021). To test for a similar pattern, we reran our allometric regression analyses excluding the 13 specimens with fewer than the adult number of 17 trunk segments. Although we were not able to determine segment numbers for a small subset of specimens in the morphometric dataset, the body lengths of all of these specimens were within the size range characterized by a stable number of 17 segments, so they were retained for these analyses.

## Results

### Taphomorphospace

**Simple Matching Distances.** Two groups of specimens were supported as optimal with k-means clustering via the Calinski-Harabasz criterion (Supplementary Fig. 5). The same two clusters are readily identified with UPGMA clustering and are visible in the PCoA (Fig. 1A, Supplementary Fig. 6). The red cluster is delimited by a long basal branch, but internally is characterized by short branches and an overall pectinate topology. The black cluster has a very short basal branch joining two to three subgroups defined by longer branches. PCo axis 1 can be seen to roughly separate the two clusters, and it shows a large eigenvalue break from higher-numbered axes in the scree plot, accounting for 46.8% of total variation. The broken stick model suggests

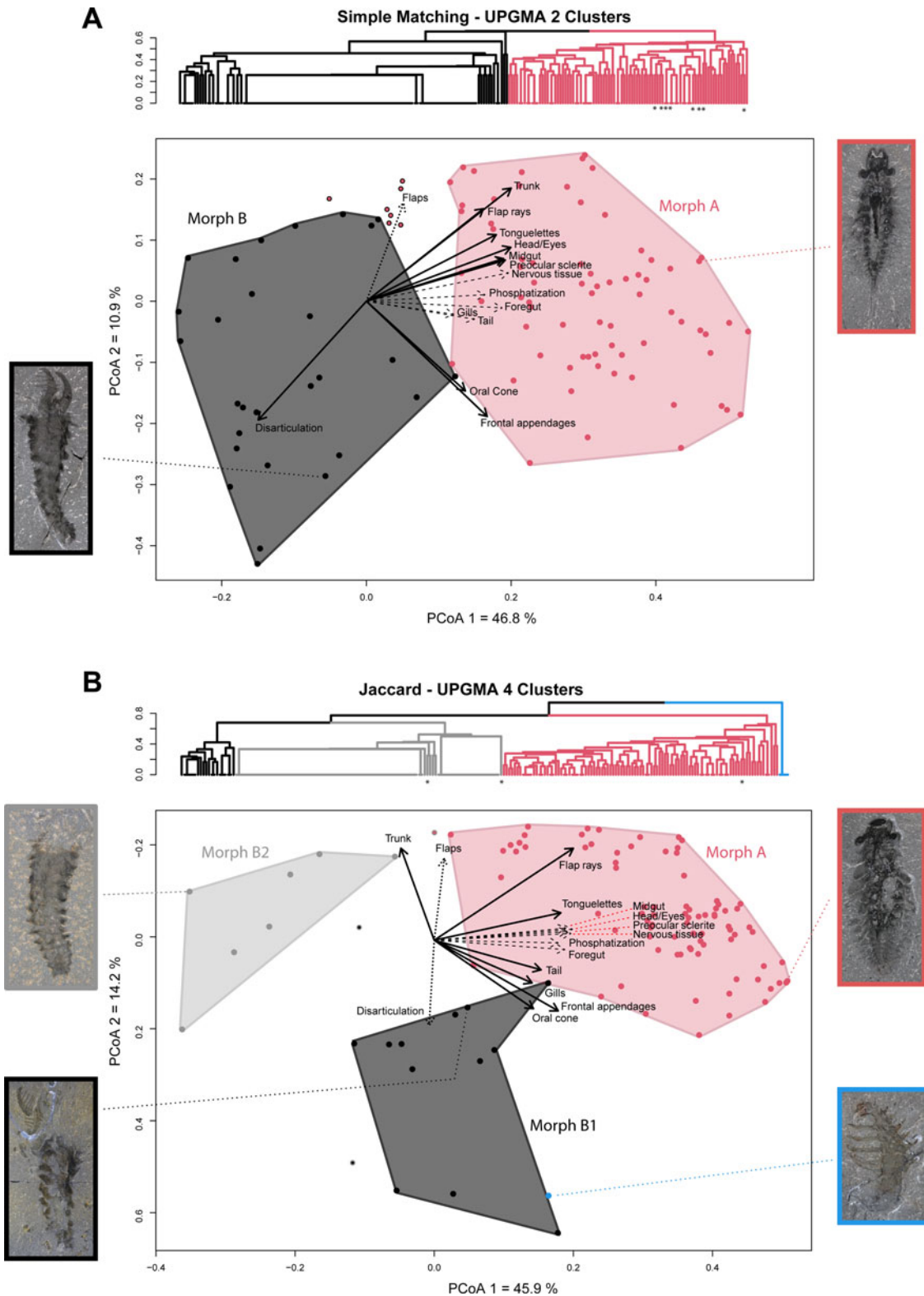


**Figure 1.** Taphomorphospace. A, Simple matching distances; B, Jaccard distances; each showing unweighted pair group method with arithmetic mean hierarchical clustering (UPGMA) cluster analysis and first two axes from principal coordinates analysis (PCoA). Optimal clusters are shown with separate colors and surrounded by convex hulls. Specimens with ambiguous cluster identity are indicated with an asterisk (\*) in the UPGMA trees and are plotted as points with two colors in the PCoA; select representative specimens are shown along left and right margins. Variable vectors are calculated to be proportional to gamma statistics calculated for each axis; dotted lines indicate significant association with the vertical axis, dashed lines with the horizontal axis, and bold lines with both axes; variables not significantly associated with either biplot axis are not represented. Axis 2 has been reversed in B to aid visual comparison. Specimen images are, from left to right, ROMIP 65754, ROMIP 65674.1, ROMIP 67532, ROMIP 65674.2, ROMIP 65755, and ROMIP 59944.

that the first 10 axes are significant, in total accounting for almost 95% of variation (Supplementary Fig. 7).

Variation between collection localities accounts for a modest, but significant amount of total variation in taphomorphospace (PERMANOVA, simple matching:  $R^2 = 0.09$ ,  $p = 0.001$ ) and appears to be significantly associated with cluster identity ( $\chi^2$ :  $p = 0.023$ ). However, this effect is driven by minor localities with few observations; when those with <5 specimens are excluded, significance is lost ( $\chi^2$ :  $p = 0.141$ ). Thus, although there is evidence for variation in taphonomic conditions between localities (Supplementary Discussion), we consider this unlikely to be the driver of the dominant clustering pattern.

The PCoA visualization with simple matching distances shows that the binary variables Trunk, Tonguelettes, Head/Eyes, Midgut, Preocular sclerite, Nervous tissue, and Foregut are strongly associated with positive values on PCo axis 1 and thus the red cluster (gamma statistics > 0.9; Fig. 1B). The variables Flap rays, Phosphatization, Oral cone, Appendages, Gills, and Tail also show weaker (gamma statistics < 0.9) but significant positive association. Disarticulation is associated with negative values on PCo 1 and the black cluster (gamma statistic = -0.75).

On higher-numbered axes, the black and red clusters are broadly overlapping, and the variable associations are more complex (Supplementary Table 1). A separation between isolated appendages and isolated trunk regions is represented on PCo 2, which is why the two corresponding variables have opposite associations with this axis. However, another pattern is superimposed—that the appendages and oral cone are actually more often observable in disarticulated assemblages (i.e., coded absent in some probable carcasses, even though they were likely present, concealed under the head). This accounts for their negative association with variables related to the head and internal tissues which can be seen when comparing the distributions of these variables over the UPGMA (Supplementary Fig. 8). This effect is somewhat reduced when considering PCo 2 from the Jaccard results, due to the treatment of shared absences with this method.

**Jaccard Distances.** Cluster analysis with Jaccard distances identifies roughly the same dominant pair of groups (only seven unambiguous disagreements; Supplementary Data 1.2), but also supports differentiation of the internal subgroupings identified in the black cluster from the simple matching results (Fig. 1B). Overall, six clusters were identified as optimal by the Calinski-Harabasz criterion; however, this solution was only slightly favored over four clusters (Supplementary Fig. 9). Further, the clustering result with six groups was similar to that with four, but included two exceedingly small groups (2 and 1 specimens) and a greater number of negative Silhouette scores. Four clusters are also readily identifiable with UPGMA clustering (Fig. 1B, Supplementary Fig. 10). We therefore favored the four-group solution.

The first 5 PCo axes are significant, accounting for greater than 80% of variation (Supplementary Fig. 11). Some specimens, particularly within the blue and gray clusters, were identical and are therefore completely overlapping in taphomorphospace (Fig. 1B). The blue cluster is readily differentiated from others, as it contains isolated appendages occupying a single point in taphomorphospace. Gray and black clusters roughly correspond to the subgroup structure seen in the black cluster with simple matching distances. The gray and black clusters are mainly differentiated from the red cluster along axis 1. Black and blue

clusters are additionally differentiated from the gray and red clusters along axis 2.

As with simple matching, locality explains a modest amount of variation in Jaccard taphomorphospace ( $R^2 = 0.12$ ,  $p = 0.001$ ) and this time is a highly significant predictor of cluster identity regardless of the inclusion of minor localities ( $p < 0.0001$ ). This difference is presumably explained by the fact that isolated appendages are here recovered in a distinct cluster (blue) from intact body remains, and the latter are nearly exclusive to the Collins Quarry localities (UE and EZ).

Variable associations with taphomorphospace axis 1 are generally similar to those seen with simple matching distances, except that Disarticulation loses its significant negative association and Trunk switches from a strong positive association to a slight, but significant negative one (Fig. 1B, Supplementary Table 2). These changes are probably driven by shifts in the placement of specimens represented by isolated trunk regions and appendages in the morphospace, as the high number of absences in these specimens makes them most sensitive to the choice of distance metric. Indeed, this is made evident by inspecting the mapping of variables over the tips of the UPGMA tree (Supplementary Fig. 12). Axis 2 primarily defines a gradient from the blue cluster, containing isolated appendages, to the gray cluster, containing isolated trunk remains. The black cluster is somewhat intermediate, containing specimens where trunk remains, appendages, and oral cones may co-occur. Specimens in the black cluster also lack the dorsal part of the head and eyes, which helped connect the appendages and trunk in life, hence they most frequently exhibit disarticulation.

Systematic variation in the red cluster is more difficult to interpret due to the lack of overt internal clustering and pectinate topology of this branch in the UPGMA. Inspection of the mapping of each character over the UPGMA (Supplementary Fig. 12) indicates that Nervous tissue, Preocular sclerite, Frontal appendages, and Foregut show the most obvious changes as one moves along the tree backbone. This pattern is somewhat less obvious with the simple matching UPGMA.

See also Supplementary Figures 13 and 14 for a sensitivity analysis excluding the variable Disarticulation.

### Description of *Stanleycaris* Morphs

The taphomorphospace results support at least two quantitatively distinct *Stanleycaris* taphomorphs, which we will refer to as Morphs A and B. Both morphs may be preserved in abundance together, for example, at Collins Quarry. Morph A (red cluster) is characterized by the presence of cuticular structures such as the dorsal part of the head and eyes, preocular sclerite, tail, and gills, as well as preservation of internal organs including nervous tissues, the gut, flap rays, and the tonguelettes (probably representing vascular lacunae and surrounding tissues; Aria et al. 2023). Phosphatization of the gills or tonguelettes may also be observed. Morph A includes the most complete specimens (e.g., Figs. 2, 3), for which a detailed description has already been provided (Moysiuk and Caron 2022). Depending on distance metric, 86 (simple matching) to 100 (Jaccard) specimens are identified as Morph A, constituting 40–46% of identifiable specimens.

Either 129 or 116 specimens are identified as Morph B (Fig. 1A, black cluster, B, black + gray clusters) by simple matching and Jaccard metrics, respectively. Morph B can be

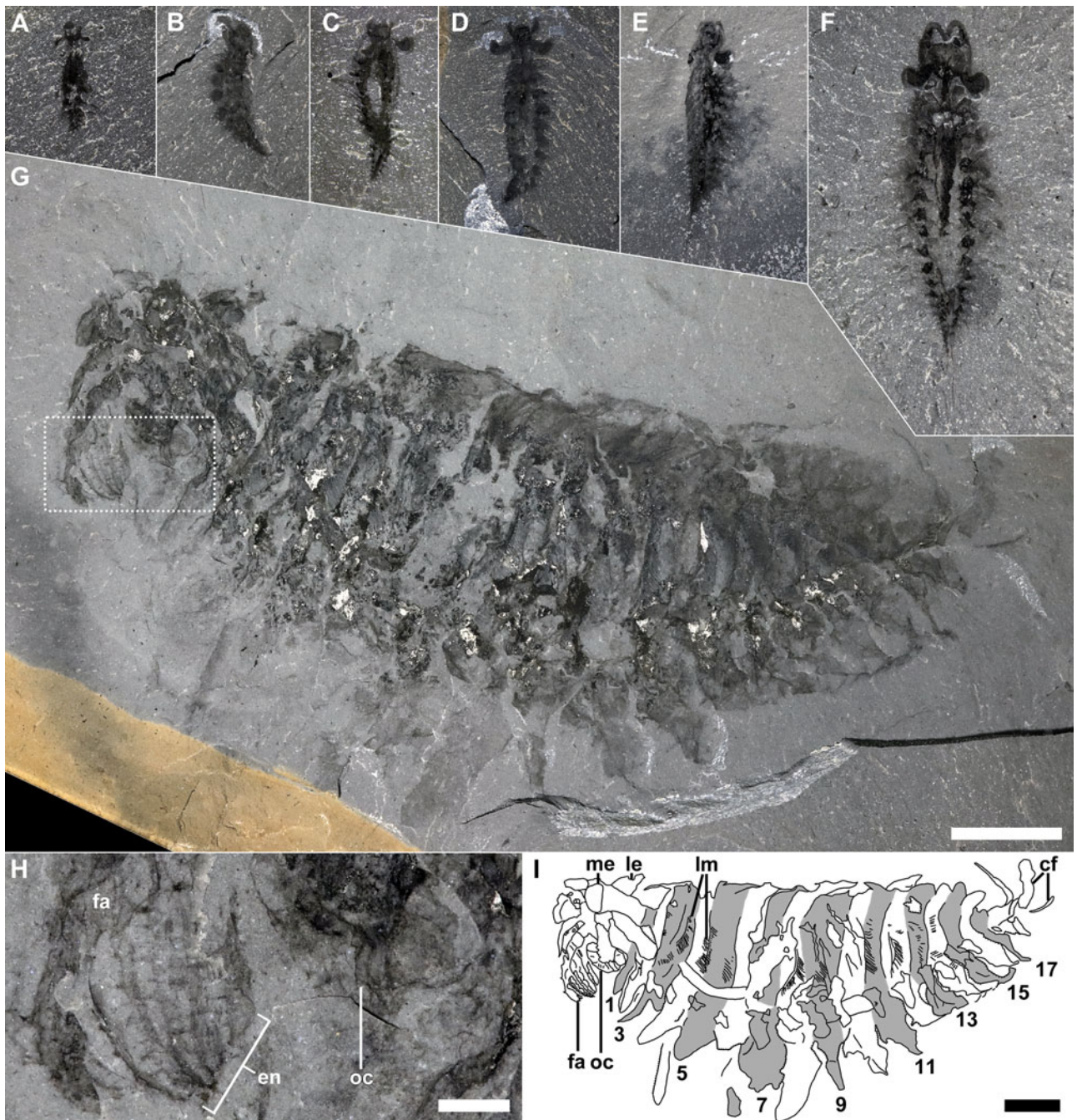


**Figure 2.** *Stanleycaris hirpex*, varied ontogenetic stages (Morph A). A, ROMIP 67533, smallest juvenile with 11 to 12 trunk segments; B, ROMIP 66902, juvenile with 12 to 13 trunk segments; C, ROMIP 65780.1, juvenile with 14 trunk segments; D, ROMIP 66903, juvenile with 14 to 15 trunk segments; E, ROMIP 65757, juvenile with 15 to 16 trunk segments; F, ROMIP 65674.1, adult with 17 trunk segments; G–I, ROMIP 65950, largest complete adult, lateral-oblique orientation: (G) overview, (H) close-up of appendages and oral cone, (I) line drawing. Scale bars, A–G: 10 mm (same scale); H: 2 mm; I: 10 mm. Abbreviations: cf, caudal filamentous blades; en, endite; fa, frontal appendage; le, lateral eye; lm, bands of gill lamellae; me, median eye; oc, oral cone; trunk segment numbers shown.

distinguished as follows. The head and some (at least 2–3) anterior trunk segments tend to be missing, with either a sharp or torn-looking boundary at the anteriormost preserved margin of the trunk (Fig. 4). The tail blades are also generally absent; the posterior trunk truncates bluntly, occasionally showing signs of overfolding or inversion (Fig. 4J, K). Parts of the trunk may be twisted or telescoped, particularly near the anterior (Fig. 4A, D, I, M). The flaps, when preserved, tend to be reduced to short lobes and may be overfolded with the body (Fig. 4). They appear

slightly darker in color than the trunk. Appendages and oral cone may be absent or present (Fig. 1B, subgroups B1 and B2, respectively), but are dislocated, often together as a unit (Fig. 4A–C, E–I, L). Internal organs appear to be absent, with the exception of a single specimen showing part of the foregut (Fig. 4C). Specimens belonging to Morph B are identifiable as *Stanleycaris* due to the diagnostic characters of their appendages and oral cones and the relatively high number of trunk segments

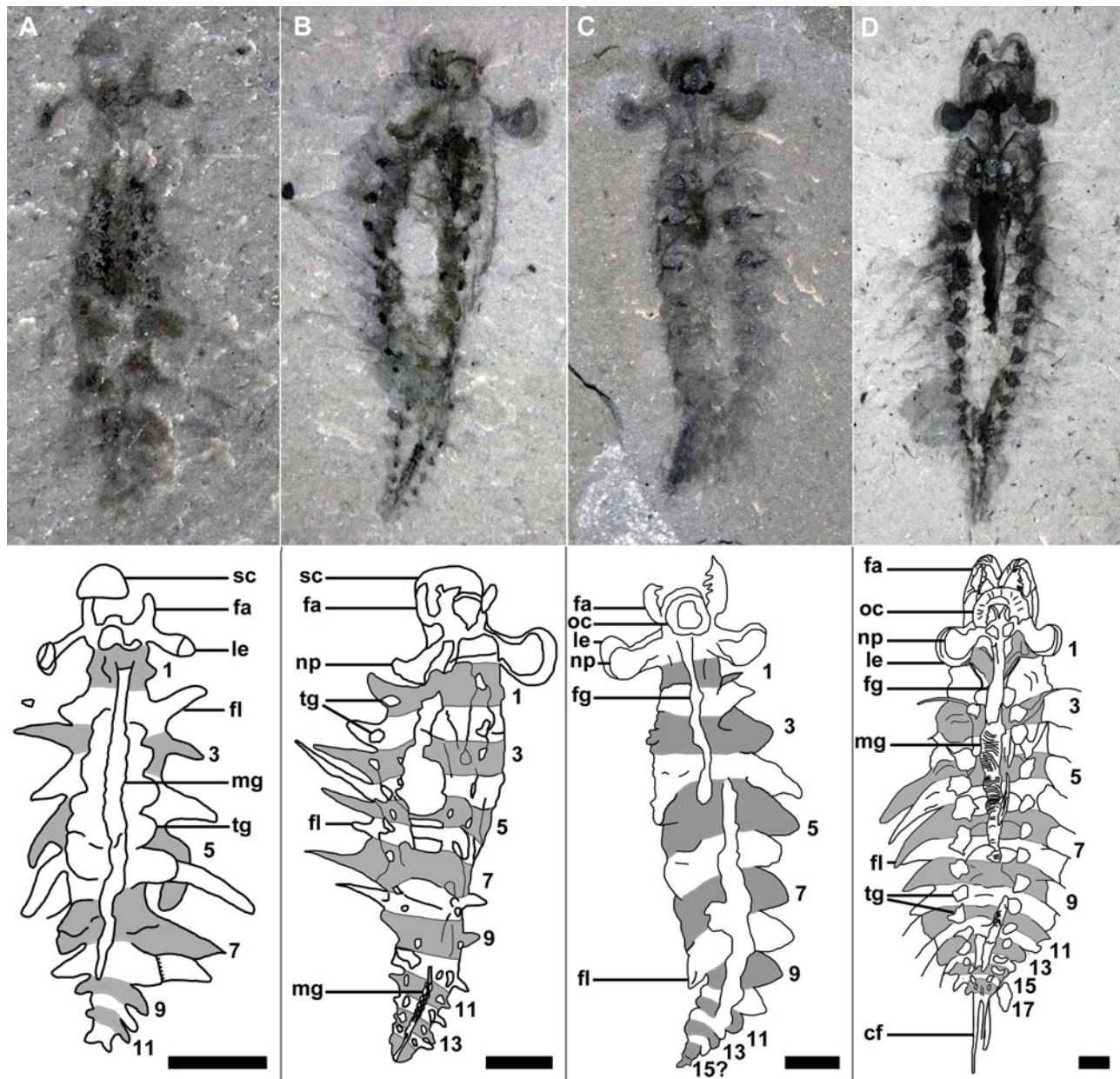


**Figure 3.** Close-ups and diagrams of select specimens from Fig. 2. A, ROMIP 67533, from Fig. 2A; B, ROMIP 65780.1, from Fig. 2C; C, ROMIP 66903, from Fig. 2D; D, ROMIP 65674.1, from Fig. 2F. Scale bars, 2 mm. Abbreviations: fg, foregut; fl, flap; mg, midgut; np, optic neuropil; sc, preocular sclerite; tg, tonguelettes; trunk segment numbers shown; all other abbreviations as in Fig. 2.

compared with co-occurring radiodont species (Moysiuk and Caron 2022).

Isolated appendages form a distinct cluster in the Jaccard taphomorphospace and could arguably be considered a third taphomorph. However, we posit that these in fact represent highly deteriorated versions of either Morph A or B that cannot be definitively placed in either group (see “Discussion”).

### Morphometrics

The smallest specimen of *Stanleyecaris* for which the number of trunk segments can be counted possesses 11 or 12 trunk segments (Figs. 2A, 3A). The number of trunk segments increases linearly with the logarithm of size up to a count of 17 (Figs. 2, 3, 5A).

Beyond this point, body size continues to increase without concomitant segment addition.

The majority of shape variables are normally distributed, with the exception of relative appendage length and oral cone diameter (Supplementary Fig. 15). This is unsurprising, as sample size was particularly low for these last two (<10) owing to the fact that few specimens are oriented in such a way as to permit reliable measurement. We therefore do not consider the bimodal distributions seen in these variables to support any sort of subpopulation structure (i.e., no dimorphism), and we did not perform further analyses with them.

Several of the remaining shape variables show an association with size. Relative eye neuropil diameter ( $r^2 = 0.47$ ,  $p = 0.001$ , allometric coefficient [AC] =  $-0.49$ ), H-element width ( $r^2 = 0.41$ ,  $p =$

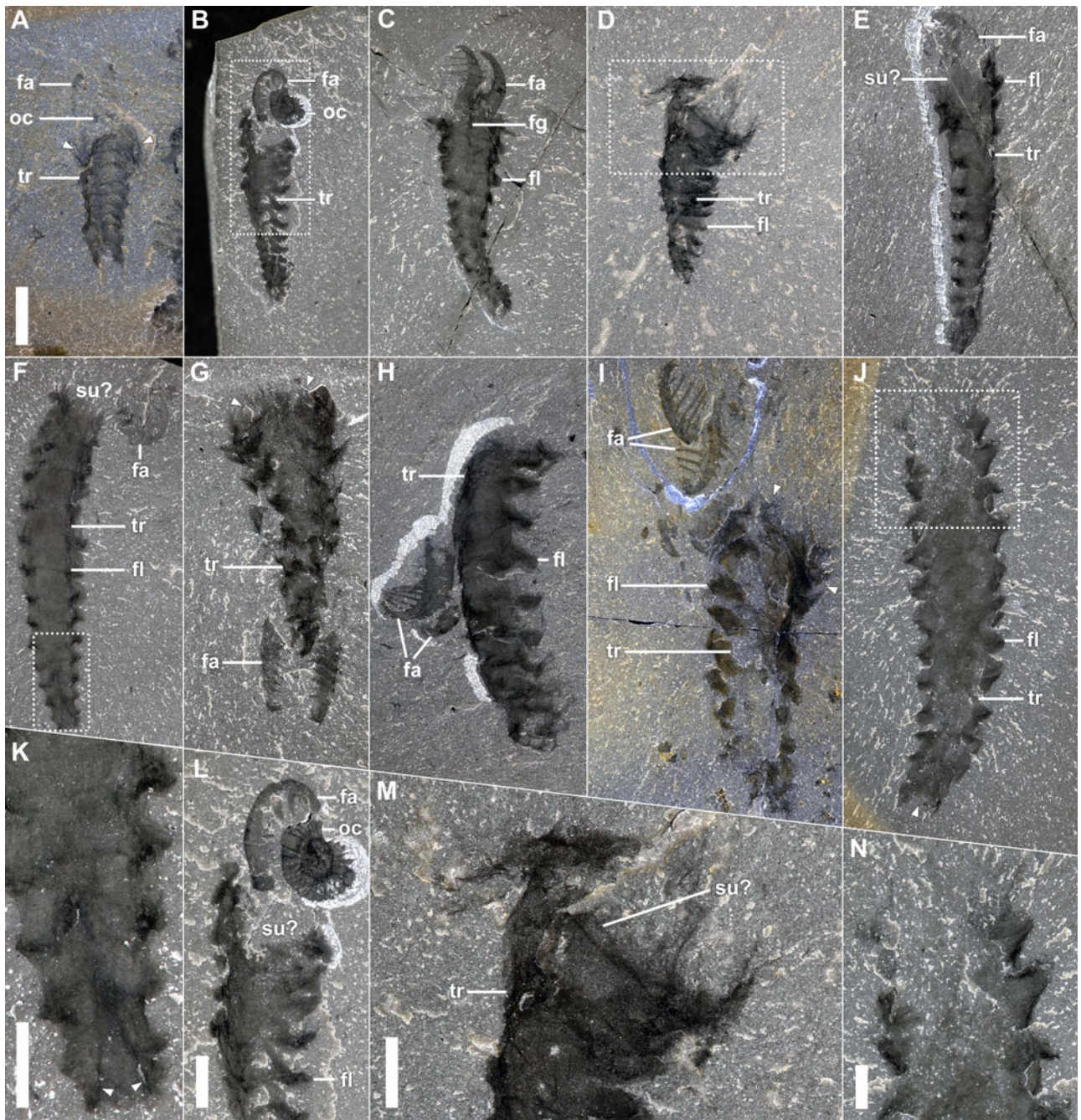


**Figure 4.** *Stanleycaris exuviae* (Morph B), showing range of variation. A, ROMIP 65771.2, arrows showing telescoping of anterior segments; B, ROMIP 65766; C, ROMIP 65754; D, ROMIP 66899, showing telescoping and breakage toward the anterior; E, ROMIP 66900; F, ROMIP 65951.2; G, ROMIP 65764.1, arrows showing breakage of anterior trunk; H, ROMIP 67534; I, ROMIP 65755, arrows showing telescoping of anterior segments; J, ROMIP 66901, arrow showing overfolded or inverted posterior termination; K, close-up from F, arrows pointing to overfolded or inverted posterior termination; L, close-up from B; M, close-up from D, showing breakage of anterior trunk; N, close-up from J, showing breakage of anterior trunk. Scale bars, A–J: 10 mm (same scale); K–N: 2 mm. Abbreviations: su?, possible molting suture; tr, trunk region; all other abbreviations as in Figs. 2, 3.

0.043, AC = 0.26), neck width ( $r^2 = 0.53$ ,  $p = 0.001$ , AC = 0.30), trunk length ( $r^2 = 0.11$ ,  $p = 0.011$ , AC = 0.02), flap length ( $r^2 = 0.13$ ,  $p = 0.015$ , AC = 0.22), and flap width ( $r^2 = 0.18$ ,  $p = 0.006$ , AC = -0.08) were found to be significantly anisometric (Fig. 5B–H). It should be noted, however, that the allometric coefficients for trunk length and flap width are also quite low, which renders their biological significance questionable. High levels of taphonomic variation due to differences in burial orientation are likely responsible for the generally low  $r^2$  values and large

confidence bands, and potentially also account for the failure to reject the null hypothesis of isometry for other shape variables (Supplementary Fig. 16). Indeed, we are unable to reject isometry for those variables that we would expect to be most impacted by burial orientation, such as relative appendage dimensions and H-element length.

When the 13 smallest specimens with fewer than the adult complement of 17 trunk segments are excluded, regression analyses generally yield comparable allometric coefficients,

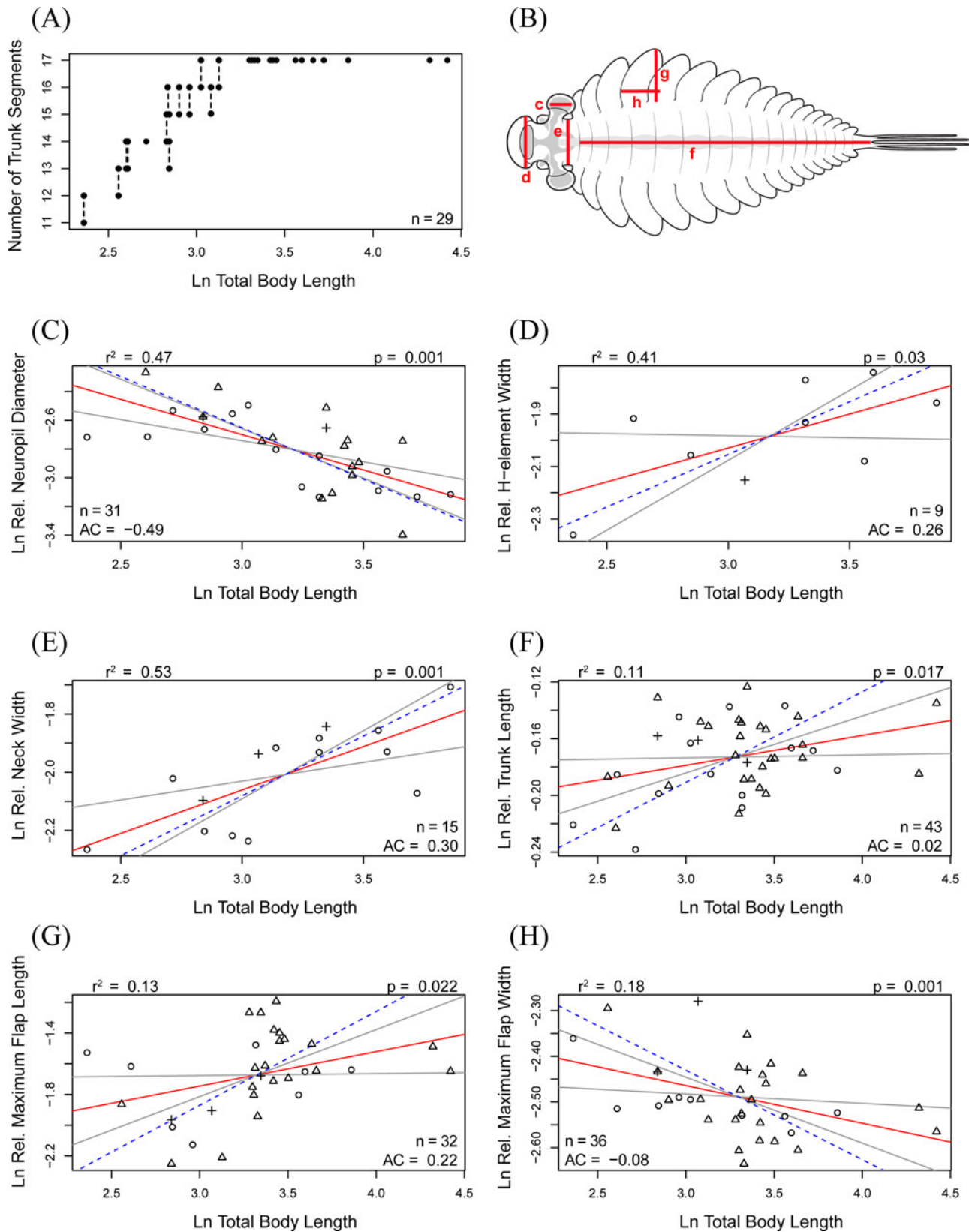


**Figure 5.** Morphometric analyses for *Stanleycaris*. A, Segment accumulation plot, showing number of trunk segments excluding terminal filiform blades; B, line drawing, with red lines representing measurements taken for each specimen, letters corresponding to subsequent figure panels, body outline by Sabrina Cappelli; C-H, shape-size biplots for each natural log-transformed shape variable listed in B. Ordinary least squares regression shown by red solid lines, with associated confidence intervals (gray) and  $r^2$ ,  $p$ -values, and allometric coefficients (AC) shown near margins, significant  $p$ -values indicating deviation from isometry. Standard major axis regression shown by blue dashed lines, point shapes indicate specimens in dorsal (open circles), ventral (plus signs), or lateral (triangles) orientation.

**Table 1.** Checklist of criteria modified from Daley and Drage (2016) used to assess evidence for putative exuvial remains of *Stanleycaris*. Criteria listed with an asterisk (\*) are the most critical.

Repeated configurations of exoskeletal parts*	<ul style="list-style-type: none"> <li>✓ Trunk region commonly cooccurring with appendages and oral cone, but head missing (Fig. 4)</li> <li>✓ Configurations quantitatively differentiated from carcasses in taphomorphospace (Fig. 1)</li> </ul>
Opened molting sutures*	<ul style="list-style-type: none"> <li>✓ Plausibly, the sharp truncations commonly observed around trunk segments 2/3 may be molt sutures (Fig. 4E,L,M).</li> <li>✓ Because appendages and oral cones may occur as a separate unit, co-occurring, but disarticulated from the trunk, they might also have separated from the head at a suture.</li> </ul>
Systematic patterns of disturbance/deformation	<ul style="list-style-type: none"> <li>✓ Disarticulation of the appendages and mouthparts, which may be shifted posterior relative to the trunk (Fig. 4A, B,F-I,L)</li> <li>✓ Reduction and shriveling of the flaps (Fig. 4)</li> <li>✓ Overfolding (Fig. 4A,F,J) and telescoping (Fig. 4A,I) of the trunk</li> <li>✓ Breakage of anterior trunk segments (Fig. 4M,N)</li> </ul>
Depositional environment	<ul style="list-style-type: none"> <li>✓ Rapid burial at the Burgess Shale minimized time averaging and postmortem disarticulation/decay of fragile structures (Caron and Jackson 2006).</li> </ul>
Absence of noncuticular structures	<ul style="list-style-type: none"> <li>✓ Midgut, nervous tissues, and “tonguelettes” (likely representing vascular lacunae; Aria et al. 2023) missing from putative exuviae, as is phosphatization (Fig. 1).</li> <li>✓ A single putative molt retains the foregut (Fig. 4C), but this is a cuticular structure that is also molted in extant ecdysozoans (Moussian 2013).</li> </ul>
Lack of evidence of predation/scavenging	<ul style="list-style-type: none"> <li>✓ Some putative molts are associated with minute surficial trace fossils (Moysiuk and Caron 2022: fig. 4G), but evidence from other taxa (e.g., <i>Tuzoia</i>, <i>Banffia</i>) suggests that their presence is probably due to the remains creating a sheltered, microbially enriched microenvironment rather than themselves being the target of scavenging (Mángano et al. 2019).</li> </ul>

but statistical significance is lost for all shape measures except relative neuropil diameter (Supplementary Fig. 17). We suggest that the change in significance may be a result of the strong signal provided by the smallest specimens (Brown and Vavrek 2015) rather than an indication of biphasic allometry.

## Discussion

### *Ecdysis in Stanleycaris and Other Radiodonts*

Radiodonts have been presumed to have undergone ecdysis during growth, as has been demonstrated for other Cambrian ecdysozoans (Daley and Drage 2016). Several authors have suggested that certain radiodont specimens may represent molts (Briggs 1979; Daley et al. 2013; Daley and Edgecombe 2014; Zeng et al. 2018; Moysiuk and Caron 2019b, 2021; Caron and Moysiuk 2021) on the basis of meeting some of the criteria outlined by Daley and Drage (2016) for distinguishing between carcasses and exuviae in the fossil record. However, distinguishing between fossil carcasses and molt remains in animals without close modern analogues is not straightforward.

Few decay experiments have considered exuvial remains, making it challenging to devise taphonomic expectations for fossils. For notostracan branchiopods, carcass morphology tends to converge toward exuvial morphology as decay proceeds and noncuticular structures are lost preferentially (Hegna 2012). Similarly, a pattern of rapid decay of internal tissues relative to the cuticle has been observed in a range of ecdysozoans (Gostling et al. 2009; Murdock et al. 2014; Sansom 2016). However, the propensity for some cuticular body parts to disarticulate differs between molts and carcasses (Hegna 2012), and other processes such as authigenic phosphatization could lead some labile tissues to persist longer than predicted by decay experiments (Parry et al. 2018). In this light, there remains potential for distinguishing carcasses and exuviae based on systematic body part associations.

Taken alongside qualitative observations of specimens (Table 1), our taphomorphospace approach provides an opportunity to identify potentially distinct preservation patterns between carcasses and exuviae. The two main clusters identified in taphomorphospace correspond to the prediction that carcasses and exuviae might exhibit as distinct taphomorphs. Accordingly, we interpret Morph A as representing carcasses and Morph B as primarily exuviae. However, before accepting this interpretation, we should consider two alternative scenarios that could conceivably generate a clustering structure in taphomorphospace.

One alternative scenario is that all labile tissues decayed rapidly and almost simultaneously, resulting in distinct clusters of carcasses of differing degrees of decay. We do not favor this as a general explanation in *Stanleycaris*, as the variables most associated with axis 1, which primarily separates the two taphomorphs, include both internal tissues and more recalcitrant cuticular features. Loss of specific cuticular elements—the head and preocular sclerite—via removal during ecdysis is a more plausible explanation. A further argument comes from phosphatization, which must have stabilized labile tissues early on and is therefore not expected to be associated with the degree of decay of non-phosphatized tissues. The fact that phosphatization is significantly and positively associated with the first axis in taphomorphospace is thus inconsistent with differential decay being responsible for the differentiation of taphomorphs.

Another process that could conceivably lead to clustering in taphomorphospace would be selective scavenging of particular structures, giving rise to systematic morphological disassociations. As is the case with rapid simultaneous decay, we find this hypothesis implausible for explaining the particular associations of internal and external morphologies. The depositional environment of the Burgess Shale also makes this less likely, as scavenging was inhibited post-burial (Caron and Jackson 2006).

Considering the results of our taphomorphospace alongside other qualitative observations (Table 1), specimens belonging to Morph B plausibly meet all criteria for identifying fossil exuviae. We must acknowledge that some putative carcasses may also lack

certain internal organs and/or phosphatization, leading to uncertain cluster assignment; however, taken in aggregate, these variables are sufficient to generate the strong divide observed between carcass and molt clusters.

In addition to the dominant clustering structure in the taphomorphospace, within-taphomorph structure is also of interest. The pectinate topology of the carcass cluster appears consistent with our expectation for a continuous decay gradient; however, upon visual identification of the variables that change systematically along the backbone (Supplementary Figs. 8, 12), we think this assessment would be inaccurate. While the losses of some of these characters, like nervous tissues and the foregut, could conceivably be due to decay, the absence of frontal appendages and the preocular sclerite are more likely due to non-observation, as these structures are expected to be the most decay resistant. This emphasizes the importance of considering patterns in taphomorphospace with different distance metrics in the context of realistic taphonomic hypotheses.

The subgrouping structure among exuviae, notably captured by the optimization of two distinct molt clusters with Jaccard distances, is of greater interest. Based on variable associations in taphomorphospace and the mapping of variables over the UPGMA trees (Supplementary Figs. 8, 12), we interpret subgroups as cases where different parts have disarticulated, resulting in sudden morphological shifts. For example, disassociation of the appendages and/or oral cone results in saltations through morphospace, as the individual parts diverge in taphonomic history thereafter. This accounts for the differentiation between molts in which the appendages or oral cone remain associated (black subgroup, “molt type 1”) and those in which they have been separated (gray, “molt type 2”). Cases of isolated appendages, and arguably appendage pairs and appendage–oral cone assemblages, are more problematic to demarcate based on the criteria for identifying exuviae (Table 1), because they would likely be the last parts lost due to progressive decay. Therefore, although these specimens may sometimes cluster together with exuviae, the case for identifying them as exuviae as opposed to extremely decayed carcass fragments must be considered inconclusive. Their conflicting assignment, either to the molt cluster or to a distinct cluster depending on distance metric, is the quantitative manifestation of this uncertainty.

The association of elements in *Stanleycaris* exuviae allows for a tentative reconstruction of its molting behavior. The observation that molts tend to be missing the preocular sclerite and dorsal head cuticle suggests that the dorsal head region was separated by a molting suture from the ventral part of the head and trunk. The trace of this suture is plausibly represented by the anterior truncated margin in these specimens. During molting, the dorsal head would have either been lost before exiting the trunk exuvium or carried away by the exiting animal. Such separate loss of elements during ecdysis is commonly seen in other fossil arthropods (Haug et al. 2013; Daley and Drage 2016) and most extremely represented by the biphasic molting mode in isopods (Sahadevan et al. 2022). The appendages and oral cone of *Stanleycaris* may remain associated with the trunk, typically disarticulated, or be entirely disassociated. We hypothesize that this can be explained by the weakening of the connection between the ventral head and trunk following separation from the dorsal head region, making it prone to breakage, though we cannot rule out the presence of an additional suture between the ventral head and trunk. Frequent reduction or lack of preservation of the flaps could be related to deformation of the cuticle as *Stanleycaris*

exited the exuvium, although it is also probably due in part simply to the thin and fragile nature of the flap cuticle, which would likewise account for poor flap preservation in carcasses.

The identification of exuviae of *Stanleycaris* has implications for understanding fossils of other radiodonts. In many derived hurdiids, putative molt assemblages frequently include head sclerites associated with appendages and oral cones, while other body parts are less commonly present (Daley et al. 2013; Moysiuk and Caron 2019b; Sun et al. 2020; Caron and Moysiuk 2021; Fig. 6B,C). This differs from the case in *Stanleycaris*, in which the preocular sclerite is typically missing while the appendages and oral cone may remain associated with the trunk. Some specimens of *Anomalocaris* (“preservational mode showing setal blades” in Daley and Edgecombe [2014]; Fig. 6A) show shriveled flaps and loss of part of the head region similar to *Stanleycaris* molts; however, in this case, the head carapace elements typically remain associated with the trunk remains (Moysiuk and Caron 2019b). If these specimens indeed represent exuviae, they are suggestive of subtle interspecific differences in the position of sutures or behavior of the exiting animal, although in all cases sutures must be positioned near the neck–trunk junction. Another peculiarity is that gill lamellae, preserved in carbonaceous mode, are only rarely visible in *Stanleycaris* exuviae, while they are frequently seen in putative equivalents in *Anomalocaris* (Daley and Edgecombe 2014). Traces of dorsal cuticular segmentation may also be effaced in exuviae of both species. We speculate that these observations could be explained by areas of extremely thin and densely imbricated cuticle tending to collapse together during decay (Hegna 2012), potentially exacerbated in *Stanleycaris* due to smaller body size. In carcasses, the gills are often associated with phosphatization (Moysiuk and Caron 2022), which is consistent with high lability and relatively rapid decay of these structures (Schiffbauer et al. 2014; Moon et al. 2021).

Beyond radiodonts, separation at the dorsal junction between the headshield or carapace is also possibly seen in Cambrian euarthropods such as megacheirans (Haug et al. 2013), fuxianhuidi (Yang et al. 2019), and some—albeit probably derived—trilobites (Daley and Drage 2016). This is similar to the severing of the cuticle of the head and neck segments from the rest of the body in *Stanleycaris* and possibly other radiodonts. The comparison with the megacheiran *Alalcomenaeus* is particularly striking, as the frontal appendages remain closely associated with the trunk even after separation of the headshield (Fig. 6D,E), which represents the dorsal expression of the first three or four postocular segments (Chen et al. 2004; Tanaka et al. 2013). These observations support the hypothesis that a suture circumscribing the dorsal cephalic region and an anterior exiting from the molt represent the ancestral mode of arthropod molting (Daley and Drage 2016) and tentatively suggest that the position of this suture, near the boundary of the ancestral euarthropod head tagma, may have been conserved among early arthropods.

The high abundance of *Stanleycaris* specimens at the Collins Quarry, especially within certain stratigraphic intervals, might be suggestive of at least sporadic grouping behavior. Moreover, small average size, clustered size distribution (Supplementary Fig. 2), and the high abundance of exuviae indicate that molting could be a plausible explanation for these aggregations. Similar behavior has been previously hypothesized for *Cambroraster* and *Anomalocaris* (O’Brien et al. 2014; Moysiuk and Caron 2019b), as well as for some Cambrian euarthropods (Haug et al. 2013; Corrales-García et al. 2020), hinting at early and widespread emergence of this strategy.

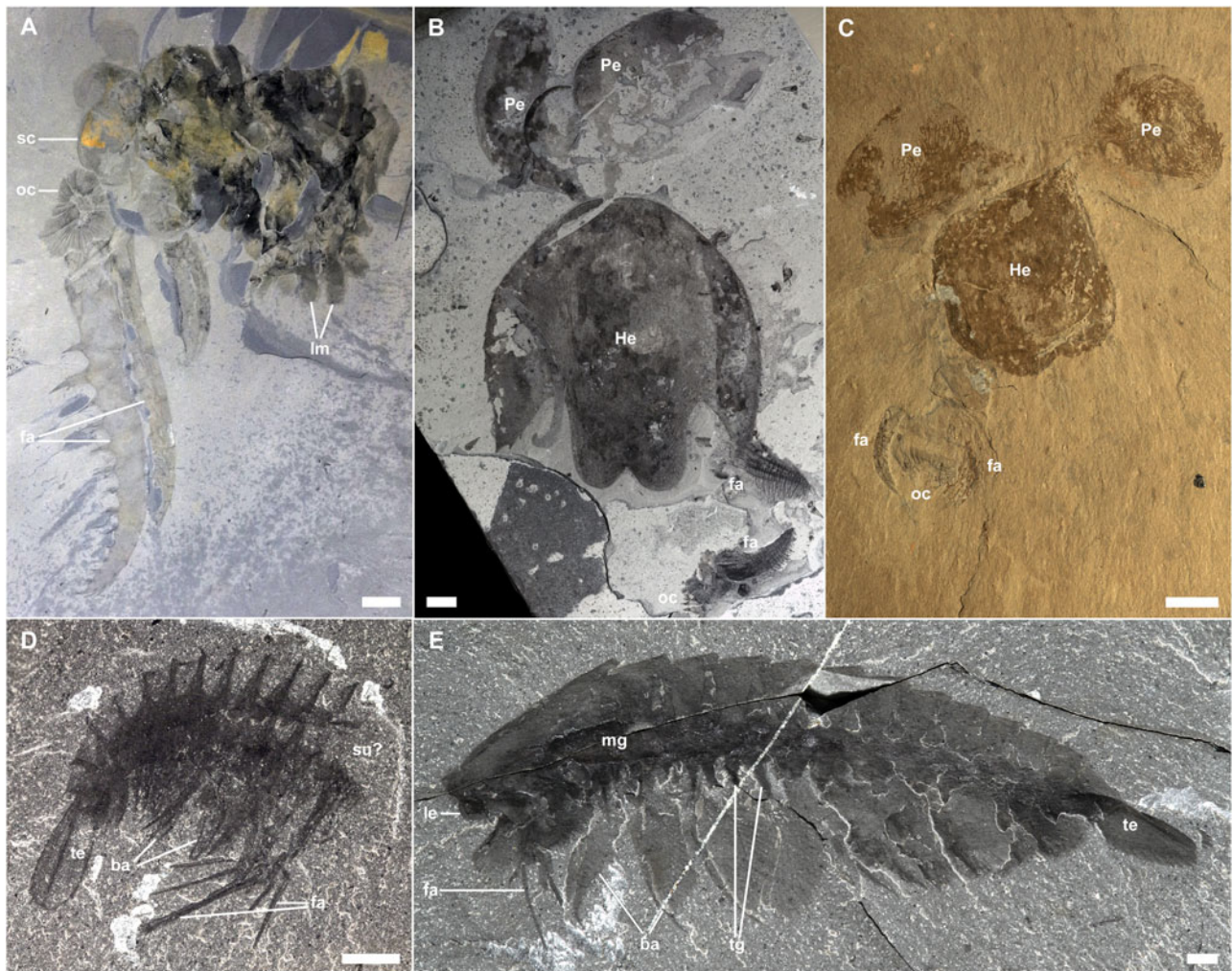


**Figure 6.** Comparative images of putative radiodont and megacheiran exuviae (except E). A, ROMIP 51215, *Anomalocaris canadensis* B, ROMIP 65079, *Cambroraster falcatus* C, ROMIP 59255, *Hurdia triangulata* D, ROMIP 57711, *Alalcomenaeus cambricus* E, ROMIP 53352, *A. cambricus*, carcass. Scale bars, A–C: 10 mm; D, E: 2 mm. Abbreviations: ba, biramous appendages; He, H-element; Pe, P-element, te, telson; all other abbreviations as in Figs. 2–4.

### Allometry

Although morphometric studies on Burgess Shale–type fossils are confounded by taphonomic influences, such as variations in burial orientation and artifacts of compression, several studies have demonstrated that biological patterns can still be teased out with careful data collection (e.g., Daley et al. 2013; Aria et al. 2015; Lunde Nielsen et al. 2017; Mayers et al. 2018; Caron and Moysiuk 2021; Zeng et al. 2021). In the case of *Stanleycaris*, the detection of patterns of allometry and segmentation benefited from the ability to exclude exuviae, which show higher levels of deformation, from our morphometric dataset.

The finding of negative allometry of the eyes of *Stanleycaris* has potential ecological significance. Several radiodont species are suggested to have been visual predators due to their large eyes, bearing huge numbers of ommatidia (Paterson et al. 2011, 2020; Moysiuk and Caron 2022). Primarily on the basis of a single small specimen of *Lyrarapax*, Liu and colleagues (Liu et al. 2018) argued that the possession of well-developed sensory and feeding organs were indicative of juveniles occupying similar visual macropredatory niches to adults, analogous to the case in living stomatopods and mantises. Data from *Stanleycaris* show that not only were lateral eyes large, but

their development was precocious relative to other body parts. Because arthropod eye size is often associated with the number and size of ommatidia, which contribute to visual acuity (Feller et al. 2021), this is supportive of an important role of vision in juveniles. Like adults (Moysiuk and Caron 2021), it is probable that juvenile *Stanleycaris* were capable of capturing active prey. However, the existence of an ecologically differentiated larval stage before the smallest ontogenetic stages in our dataset cannot yet be ruled out (see “Segment Addition”).

More generally, it is of interest to consider the potential impact of allometry on evolution in radiodonts. Presently, the lack of comparative data from other species makes it premature to draw conclusions about heterochrony, but it is possible to make speculative predictions by making the simplifying assumption that the allometries observed in *Stanleycaris* were broadly conservative.

Derived hurdiids, exemplified by *Cambroraster*, are characterized by enlarged heads and head carapaces relative to their bodies and a broadening of the neck region such that the head–trunk boundary is effaced (Moysiuk and Caron 2019b). In *Stanleycaris*, the neck and H-element become relatively broader with increasing size. This could hint that peramorphosis played

a role in the evolution of the distinctive heads of derived hurdiids. Possible support for allometric conservatism comes from the positive association between relative H-element width and size in *Cambroraster* (Caron and Moysiuk 2021). However, a caveat is that the use of H-element centroid size rather than total body length as the size variable in that study means that the allometries are not directly comparable.

By contrast, relative trunk length and adult number of trunk segments in derived hurdiids are considerably reduced relative to *Stanleycaris*, anomalocaridids, and amplexobeluids. These traits could have evolved via paedomorphosis, assuming conservation of the putative slightly positive allometry in relative trunk length in *Stanleycaris*. Similarly, the short and broad flaps of derived hurdiids could have evolved via paedomorphosis from an ontogenetic trajectory in which the flaps become progressively longer and narrower, as tentatively seen in *Stanleycaris*. If the aforementioned contrasting patterns of heterochrony in the head and trunk regions can be supported, the implication will be that the origin of the distinctive hurdiid body plan involved mosaic heterochrony (sensu Gerber and Hopkins 2011). Such predictions must remain speculative for now, as only further discoveries of ontogenetic series of other radiodont species can allow testing of the assumption of conserved allometry upon which they rest.

### Segment Addition

Development in panarthropods can be classified as either epimorphic—in which segments are added in the embryonic period—or anamorphic—in which segment addition continues in the post-embryonic period (Fusco and Minelli 2021). These two are not mutually exclusive, as many species undergo distinct anamorphic and epimorphic growth phases, that is, hemianamorphosis.

Well-preserved *Stanleycaris* juveniles presented in this paper offer the first glimpse of segment development in a radiodont. The smallest postembryonic instars of *Stanleycaris* presumably remain unknown, such that the number of segments in hatchlings is ambiguous. It is also not possible to determine whether radiodonts had a strictly defined larval stage, as has been reported, for example, in leanchoiliid megacheirans (Aria et al. 2015; Liu et al. 2016). The smallest known juvenile, ca. 10 mm, possesses only 11 or 12 trunk segments, not including the caudal filiform blades. From this instar, the number of trunk segments increases, presumably by subterminal addition, up to a body length of about 20 mm, at which point segment number stabilizes at 17. Maximum body size excluding tail blades reaches at least 83 mm based on complete specimens and probably as large as ca. 180 mm based on extrapolation from isolated appendages, assuming a constant ratio of appendage length to body length. Exuviae larger than the size at which segment addition was terminated (Fig. 4) demonstrate the existence of an epimorphic phase. The described pattern therefore represents a compelling case of hemianamorphic development.

Hemianamorphic development, with new segments generated from a posterior segment addition zone, is widespread in euarthropods and has been generally held to be ancestral for the phylum (Waloszek and Maas 2005; Fusco and Minelli 2021). Hemianamorphosis is found in virtually every major group of Cambrian euarthropods, including trilobites (Hughes et al. 2021), marrellomorphs (García-Bellido and Collins 2006), megacheirans (Liu et al. 2014), isoxyids (Fu et al. 2014), fuxianhuiids (Fu et al. 2018), pancrustaceans (Waloszek and Maas 2005; Hug et al. 2014), and probably hymenocarines

(Izquierdo-López and Caron 2021; Liu et al. 2022). By contrast with euarthropods, tardigrade development is epimorphic, with all segments arising roughly simultaneously during embryogenesis (Smith and Goldstein 2017; but see Maas and Waloszek [2001] for a possible Cambrian exception). Onychophorans also exhibit epimorphic development, as newborns or hatchlings emerge with a full complement of segments, although unlike in tardigrades, new segments are sequentially added during embryogenesis in a posterior segment addition zone (Mayer et al. 2015). While the relationships of these three panarthropod phyla remain contested, it is likely that either onychophorans or tardigrades are the closest extant relatives of euarthropods (Giribet and Edgecombe 2017). Altogether, this implies that either epimorphosis is the ancestral mode of segment development in Panarthropoda or, less parsimoniously, that it evolved convergently in tardigrades and onychophorans. The fossil record is also tentatively consistent with ancestral epimorphosis, as Cambrian lobopodians like *Hallucigenia* show no evidence of segment addition during known ontogenetic stages (Smith and Caron 2015). However, it admittedly remains possible that segment addition in lobopodians occurred in minute juvenile or larval stages that have yet to be discovered.

Radiodonts are the sister clade to the remainder of Arthropoda (Daley et al. 2009; Moysiuk and Caron 2022), making them highly significant for understanding the timing and polarization of morphological transitions at the origin of the arthropod body plan. The observation that *Stanleycaris* added segments up to a stable maximum during the postembryonic period serves to further solidify the hypothesis that a hemianamorphic mode of development was ancestral for arthropods. More importantly, this finding is significant in helping to refine the timing of the origin of this important developmental trait. If epimorphosis is indeed ancestral for Panarthropoda as a whole, hemianamorphosis must have evolved in the euarthropod stem group, before the radiodont-euarthropod split. This transition from epimorphosis to hemianamorphosis would then represent an exceedingly rare case (Fusco and Minelli 2021), arguably a release from developmental constraint near the origin of Arthropoda.

### Conclusions

New collections of *Stanleycaris* make up the most complete known ontogenetic series for a radiodont, providing a record of ecdysis, allometric changes during growth, and hemianamorphic development. Exuviae of *Stanleycaris* can be identified by a combination of qualitative and quantitative criteria, confirming that radiodonts grew by periodic ecdysis, as expected given their arthropod affinity. The taphomorphospace approach developed here provides a new quantitative tool to aid in the rigorous assessment of molting in the fossil record and should be applicable in other cases, particularly when exceptional preservation has occurred. The pattern of exuviation in *Stanleycaris* and related species suggests that a molting suture circumscribing the first few anterior segments is likely ancestral for arthropods. The fact that this discrete anterior segmental unit apparently corresponds to the ancestral euarthropod head tagma provides an intriguing hint that this batch of segments began to differentiate subtly before undergoing fusion and cephalic integration. The discovery of hemianamorphosis in a radiodont supports the notion that this developmental mode is ancestral for arthropods, and these new findings constrain its likely origin point to a position deep in the euarthropod stem group. Taken together, these discoveries

represent an important first step in understanding the developmental paleobiology of radiodonts. Great potential remains for new fossil discoveries to yield insights about radiodont ontogeny and the role of development in the evolution of the earliest arthropods.

**Acknowledgments.** We thank M. Hopkins, S. Pates, and two anonymous reviewers for challenging us to make the most of our analyses. J.M. would like to thank D. Jackson for helpful comments, in particular during the course Multivariate Statistics (EEB1230); A. Izquierdo-Lopez for assistance with R code and general remarks; and S. Kvist, M. Laflamme, T. Lowi-Merri, C. Aria, and H. Osawa for helpful discussions. Comments and suggestions from members of the “PaleoClub” at the University of Lausanne, Switzerland, also stimulated important improvements. We thank M. Akrami for assistance with the ROMIP collections and S. Cappelli for artistic reconstructions. Funding comes primarily from a Natural Sciences and Engineering Research Council (NSERC) Discovery grant (no. 341944) to J.-B.C. and an NSERC Vanier Canada Graduate Scholarship, Ontario Graduate Scholarship, and Martin Scholarship to J.M., through the Department of Ecology and Evolutionary Biology, University of Toronto. The fossil material of *Stanleycaris* featured in this paper was collected under several Parks Canada Research and Collecting permits to the late D. Collins. This is Royal Ontario Museum Burgess Shale Project 96.

**Competing Interests.** The authors declare no competing interests.

**Data Availability Statement.** Supplementary Discussion, Figures, and Data for this study, including morphometric data, the matrix of characters used for taphomorphospace construction, and R code, are available in the Dryad Digital Repository: <https://doi.org/10.5061/dryad.gqnk98stj>.

## Literature Cited

- Aria, C. 2020. Macroevolutionary patterns of body plan canalization in euarthropods. *Paleobiology* 46:569–593.
- Aria, C., and J.-B. Caron. 2017. Burgess Shale fossils illustrate the origin of the mandibulate body plan. *Nature* 545:89–92.
- Aria, C., J.-B. Caron, and R. Gaines. 2015. A large new leaenchoiliid from the Burgess Shale and the influence of inapplicable states on stem arthropod phylogeny. *Palaeontology* 58:629–660.
- Aria, C., J. Vannier, T.-Y. S. Park, and R. R. Gaines. 2023. Interpreting fossilized nervous tissues. *BioEssays* 45:2200167.
- Briggs, D. E. G. 1979. *Anomalocaris*: the largest known Cambrian arthropod. *Palaeontology* 22:631–664.
- Brown, C. M., and M. J. Vavrek. 2015. Small sample sizes in the study of ontogenetic allometry; implications for palaeobiology. *PeerJ* 3:e818.
- Caron, J. B., and D. A. Jackson. 2006. Taphonomy of the Greater Phyllopod Bed community, Burgess Shale. *Palaios* 21:451–465.
- Caron, J.-B. 2005. *Banffia constricta*, a putative vetulicolid from the Middle Cambrian Burgess Shale. *Transactions of the Royal Society of Edinburgh (Earth Sciences and Environmental Science)* 96:95–111.
- Caron, J.-B., and J. Moysiuk. 2021. A giant nektobenthic radiodont from the Burgess Shale and the significance of hurdiid carapace diversity. *Royal Society Open Science* 8:210664.
- Caron, J.-B., R. R. Gaines, M. G. Mángano, M. Streng, and A. C. Daley. 2010. A new Burgess Shale-type assemblage from the “thin” Stephen Formation of the southern Canadian Rockies. *Geology* 38:811–814.
- Chen, J., D. Waloszek, and A. Maas. 2004. A new “great-appendage” arthropod from the Lower Cambrian of China and homology of chelicerate chelicerae and raptorial antero-ventral appendages. *Lethaia* 37:3–20.
- Chipman, A. D., and G. D. Edgecombe. 2019. Developing an integrated understanding of the evolution of arthropod segmentation using fossils and evo-devo. *Proceedings of the Royal Society of London B* 286:20191881.
- Corrales-García, A., J. Esteve, Y. Zhao, and X. Yang. 2020. Synchronized moulting behaviour in trilobites from the Cambrian Series 2 of South China. *Scientific Reports* 10:14099.
- Daley, A. C., and H. B. Drage. 2016. The fossil record of ecdysis, and trends in the moulting behaviour of trilobites. *Arthropod Structure and Development* 45:71–96.
- Daley, A. C., and G. D. Edgecombe. 2014. Morphology of *Anomalocaris canadensis* from the Burgess Shale. *Journal of Paleontology* 88:68–91.
- Daley, A. C., G. E. Budd, J.-B. Caron, G. D. Edgecombe, and D. Collins. 2009. The Burgess Shale anomalocaridid *Hurdia* and its significance for early euarthropod evolution. *Science* 323:1597–1600.
- Daley, A. C., G. E. Budd, and J.-B. Caron. 2013. Morphology and systematics of the anomalocaridid arthropod *Hurdia* from the Middle Cambrian of British Columbia and Utah. *Journal of Systematic Palaeontology* 11:743–787.
- Daley, A. C., J. B. Antcliffe, H. B. Drage, and S. Pates. 2018. Early fossil record of Euarthropoda and the Cambrian Explosion. *Proceedings of the National Academy of Sciences USA* 115:5323–5331.
- Dray, S., and A. B. Dufour. 2007. The ade4 package: implementing the duality diagram for ecologists. *Journal of Statistical Software* 22:1–20.
- Edgecombe, G. D. 2020. Arthropod origins: integrating paleontological and molecular evidence. *Annual Review of Ecology, Evolution, and Systematics* 51:1–25.
- Eriksson, M. E., and F. Terfelt. 2012. Exceptionally preserved Cambrian trilobite digestive system revealed in 3D by synchrotron-radiation X-ray tomographic microscopy. *PLoS ONE* 7:e35625.
- Eriksson, M. E., and D. Waloszek. 2016. Half-a-billion-year-old microscopic treasures—the Cambrian “Orsten” fossils of Sweden. *Geology Today* 32:115–120.
- Feller, K. D., C. R. Sharkey, A. McDuffee-Altekruse, H. D. Bracken-Grissom, N. P. Lord, M. L. Porter, and L. E. Schweikert. 2021. Surf and turf vision: patterns and predictors of visual acuity in compound eye evolution. *Arthropod Structure and Development* 60:101002.
- Fletcher, T. P., and D. H. Collins. 1998. The Middle Cambrian Burgess Shale and its relationship to the Stephen Formation in the southern Canadian Rocky Mountains. *Canadian Journal of Earth Sciences* 35:413–436.
- Foote, M. 1995. Morphology of Carboniferous and Permian crinoids. *Contributions from the Museum of Paleontology University of Michigan* 29:135–184.
- Friendly, M. 2022. vcdExtra: “vcd” extensions and additions. <https://friendly.github.io/vcdExtra>, accessed 1 November 2022.
- Fu, D., X. Zhang, G. E. Budd, W. Liu, and X. Pan. 2014. Ontogeny and dimorphism of *Isoxys auritus* (Arthropoda) from the Early Cambrian Chengjiang biota, South China. *Gondwana Research* 25:975–982.
- Fu, D., J. Ortega-Hernández, A. C. Daley, X. Zhang, and D. Shu. 2018. Anamorphic development and extended parental care in a 520 million-year-old stem-group euarthropod from China. *BMC Evolutionary Biology* 18:1–17.
- Fusco, G., and A. Minelli. 2021. The development of arthropod segmentation across the embryonic/post-embryonic divide—An evolutionary perspective. *Frontiers in Ecology and Evolution* 9:622482.
- Galili, T. 2015. dendextend: an R package for visualizing, adjusting and comparing trees of hierarchical clustering. *Bioinformatics* 31:3718–3720.
- García-Bellido, D. C., and D. H. Collins. 2006. A new study of *Marrella splendens* (Arthropoda, Marrellomorpha) from the Middle Cambrian Burgess Shale, British Columbia, Canada. *Canadian Journal of Earth Sciences* 43:721–742.
- Gerber, S., and M. J. Hopkins. 2011. Mosaic heterochrony and evolutionary modularity: the trilobite genus *Zacanthopsis* as a case study. *Evolution* 65:3241–3252.
- Giribet, G., and G. D. Edgecombe. 2017. Current understanding of Ecdysozoa and its internal phylogenetic relationships. *Integrative and Comparative Biology* 57:455–466.
- Gostling, N. J., X. Dong, and P. C. J. Donoghue. 2009. Ontogeny and taphonomy: an experimental taphonomy study of the development of the brine shrimp *Artemia salina*. *Palaeontology* 52:169–186.
- Gould, S. J. 1989. *Wonderful life*. Norton, New York.
- Haug, C., J. T. Haug, A. Maas, and D. Waloszek. 2014. Fossil larvae (head larvae, nauplii, and others) from the Cambrian in Orsten preservation. Pp. 17–21 in J. W. Martin, J. Olesen, and J. T. Hoeg, eds. *Atlas of crustacean larvae*. Johns Hopkins University Press, Baltimore, Md.
- Haug, J. T., A. Maas, C. Haug, and D. Waloszek. 2011. *Sarotrocercus oblitus*—small arthropod with great impact on the understanding of arthropod evolution? *Bulletin of Geosciences* 86:725–736.

- Haug, J. T., J.-B. Caron, and C. Haug. 2013. Demecology in the Cambrian: synchronized molting in arthropods from the Burgess Shale. *BMC Biology* 11:64.
- Hedrick, B. P., and P. Dodson. 2013. Lujiatun psittacosaurids: understanding individual and taphonomic variation using 3D geometric morphometrics. *PLoS ONE* 8:e69265.
- Hegna, T. A. 2012. Phylogeny and fossil record of branchiopod crustaceans: an integrative approach. PhD thesis. Yale University, New Haven, Conn.
- Holmes, J. D., J. R. Paterson, and D. C. García-Bellido. 2021. Complex axial growth patterns in an early Cambrian trilobite from South Australia. *Proceedings of the Royal Society of London B* 288. <https://doi.org/10.1098/rspb.2021.2131>.
- Hopkins, M. J. 2016. Magnitude versus direction of change and the contribution of macroevolutionary trends to morphological disparity. *Biological Journal of the Linnean Society* 118:116–130.
- Hopkins, M. J. 2017. Development, trait evolution, and the evolution of development in trilobites. *Integrative and Comparative Biology* 57:488–498.
- Hughes, N. C. 2007. The evolution of trilobite body patterning. *Annual Review of Earth and Planetary Sciences* 35:401–434.
- Hughes, N. C., J. M. Adrain, J. D. Holmes, P. S. Hong, M. J. Hopkins, J. B. Hou, A. Minelli, T. Y. S. Park, J. R. Paterson, J. Peng, M. Webster, X. G. Zhang, X. L. Zhang, and G. Fusco. 2021. Articulated trilobite ontogeny: suggestions for a methodological standard. *Journal of Paleontology* 95:298–304.
- Izquierdo-López, A., and J.-B. Caron. 2021. A Burgess Shale mandibulate arthropod with a pygidium: a case of convergent evolution. *Papers in Palaeontology* 7:1877–1894.
- Jackson, D. A. 1993. Stopping rules in principal components analysis: a comparison of heuristic and statistical approaches. *Ecology* 74:2204–2214.
- Kilmer, J. T., and R. L. Rodríguez. 2017. Ordinary least squares regression is indicated for studies of allometry. *Journal of Evolutionary Biology* 30:4–12.
- Legendre, P. 2018. lmodel2: Model II regression. <https://cran.r-project.org/web/packages/lmodel2/index.html>, accessed 1 November 2022.
- Liu, C., D. Fu, and X. Zhang. 2022. Developmental dynamics is revealed in the early Cambrian arthropod *Chuanodianella ovata*. *iScience* 25:103591.
- Liu, J., R. Lerosey-Aubril, M. Steiner, J. A. Dunlop, S. Degan, and J. R. Paterson. 2018. Origin of raptorial feeding in juvenile euarthropods revealed by a Cambrian radiodont. *National Science Review* 5:863–869.
- Liu, Y., J. T. Haug, C. Haug, D. E. G. Briggs, and X. Hou. 2014. A 520 million-year-old chelicerate larva. *Nature Communications* 2014 5:4440.
- Liu, Y., R. R. Melzer, J. T. Haug, C. Haug, D. E. G. Briggs, M. K. Hörnig, Y. Y. He, and X. G. Hou. 2016. Three-dimensionally preserved minute larva of a great-appendage arthropod from the early Cambrian Chengjiang biota. *Proceedings of the National Academy of Sciences USA* 113:5542–5546.
- Lloyd, G. T. 2016. Estimating morphological diversity and tempo with discrete character-taxon matrices: implementation, challenges, progress, and future directions. *Biological Journal of the Linnean Society* 118:131–151.
- Lunde Nielsen, M., J. A. Rasmussen, and D. A. T. Harper. 2017. Sexual dimorphism within the stem-group arthropod *Isoxys volucris* from the Sirius Passet Lagerstätte, North Greenland. *Bulletin of the Geological Society of Denmark* 65:47–58.
- Maas, A., and D. Waloszek. 2001. Cambrian derivatives of the early Arthropod stem lineage, Pentastomids, tardigrades and Lobopodians—an “Orsten” perspective. *Zoologischer Anzeiger* 240:451–459.
- Maechler, M., P. Rousseeuw, A. Struyf, M. Hubert, and K. Hornik. 2019. cluster: cluster analysis basics and extensions. <https://CRAN.R-project.org/package=cluster>, accessed 1 November 2022.
- Mángano, M. G., C. D. Hawkes, and J.-B. Caron. 2019. Trace fossils associated with Burgess Shale non-biomineralized carapaces: bringing taphonomic and ecological controls into focus. *Royal Society Open Science* 6:172074.
- Mayer, G., F. A. Franke, S. Treffkorn, V. Gross, and I. de S. Oliveira. 2015. Onychophora. Pp. 53–98 in *Evolutionary developmental biology of invertebrates 3: Ecdysozoa I: Non-Tetraconata*. Springer, Vienna.
- Mayers, B., C. Aria, and J.-B. Caron. 2018. Three new naraoiid species from the Burgess Shale, with a morphometric and phylogenetic reinvestigation of Naraoiidae. *Palaeontology* 62:1–32.
- Meyer, D., A. Zeileis, and K. Hornik. 2007. The strucplot framework: visualizing multi-way contingency tables with vcd. *Journal of Statistical Software* 17:1–48.
- Moon, J., J.-B. Caron, and R. R. Gaines. 2021. Synchrotron imagery of phosphatized eggs in *Waptia* cf. *fieldensis* from the middle Cambrian (Miaolingian; Wuliuan) Spence Shale of Utah. *Journal of Paleontology* 96:152–163.
- Moussian, B. 2013. The arthropod cuticle. Pp. 171–196 in *Arthropod biology and evolution: molecules, development, morphology*. Springer, Berlin.
- Moysiuk, J., and J.-B. Caron. 2019a. Burgess Shale fossils shed light on the agnostid problem. *Proceedings of the Royal Society of London B* 286:20182314.
- Moysiuk, J., and J.-B. Caron. 2019b. A new hurdiid radiodont from the Burgess Shale evinces the exploitation of Cambrian infaunal food sources. *Proceedings of the Royal Society of London B* 286:20191079.
- Moysiuk, J., and J.-B. Caron. 2021. Exceptional multifunctionality in the feeding apparatus of a mid-Cambrian radiodont. *Paleobiology* 47:704–724.
- Moysiuk, J., and J.-B. Caron. 2022. A three-eyed radiodont with fossilized neuroanatomy informs the origin of the arthropod head and segmentation. *Current Biology* 32:3302–3316.
- Murdock, D. J. E., S. E. Gabbott, G. Mayer, and M. A. Purnell. 2014. Decay of velvet worms (Onychophora), and bias in the fossil record of lobopodians. *BMC Evolutionary Biology* 14:1–10.
- O'Brien, L. J., J.-B. Caron, and R. R. Gaines. 2014. Taphonomy and depositional setting of the Burgess Shale Tulip Beds, Mount Stephen, British Columbia. *Palaios* 29:309–324.
- Oksanen, J., F. G. Blanchet, M. Friendly, R. Kindt, P. Legendre, D. McGlenn, P. R. Minchin, R. B. O'Hara, G. L. Simpson, P. Solymos, M. Henry, H. Stevens, E. Szoecs, and H. W. Maintainer. 2020. vegan: community ecology, R package version 2.5-7. <https://github.com/vegandevs/vegan>, accessed 1 November 2022.
- Parry, L. A., F. Smithwick, K. K. Nordén, E. T. Saitta, J. Lozano-Fernandez, A. R. Tanner, J. B. Caron, G. D. Edgecombe, D. E. G. Briggs, and J. Vinther. 2018. Soft-bodied fossils are not simply rotten carcasses—toward a holistic understanding of exceptional fossil preservation. *BioEssays* 40:1700167.
- Paterson, J. R., D. C. García-Bellido, M. S. Y. Lee, G. A. Brock, J. B. Jago, and G. D. Edgecombe. 2011. Acute vision in the giant Cambrian predator *Anomalocaris* and the origin of compound eyes. *Nature* 480:237–240.
- Paterson, J. R., G. D. Edgecombe, and D. C. García-Bellido. 2020. Disparate compound eyes of Cambrian radiodonts reveal their developmental growth mode and diverse visual ecology. *Science Advances* 6:eabc6721.
- Raff, R. A. 2007. Written in stone: fossils, genes and evo–devo. *Nature Reviews Genetics* 8:911–920.
- R Core Team. 2020. R: a language and environment for statistical computing. R Foundation for Statistical Computing, Vienna.
- Sahadevan, A. V., J. P. T. A., and S. Kappalli. 2022. Biphasic moulting in isopods confers advantages for their adaptation to various habitats and life-style. *Biologia* 77:1067–1081.
- Saleh, F., J. B. Antcliffe, B. Lefebvre, B. Pittet, L. Laibl, F. Perez Peris, L. Lustrì, P. Gueriau, and A. C. Daley. 2020. Taphonomic bias in exceptionally preserved biotas. *Earth and Planetary Science Letters* 529:115873.
- Sansom, R. S. 2016. Preservation and phylogeny of Cambrian ecdysozoans tested by experimental decay of *Priapulid*. *Scientific Reports* 6:1–12.
- Schiffbauer, J. D., A. F. Wallace, J. Broce, and S. Xiao. 2014. Exceptional fossil conservation through phosphatization. *Paleontological Society Papers* 20:59–82.
- Schneider, C. A., W. S. Rasband, and K. W. Eliceiri. 2012. NIH Image to ImageJ: 25 years of image analysis. *Nature Methods* 9:671–675.
- Shipunov, A., P. Murrell, M. D'Orazio, S. Turner, E. Altshuler, M. W. Beck, S. Gibb, Weiliang Qiu, E. Paradis, R. Roger Koenker, and R Core Team. 2022. shipunov: miscellaneous functions from Alexey Shipunov. <https://CRAN.R-project.org/package=shipunov>, accessed 1 November 2022.
- Smith, F. W., and B. Goldstein. 2017. Segmentation in Tardigrada and diversification of segmental patterns in Panarthropoda. *Arthropod Structure and Development* 46:328–340.
- Smith, M. R., and J.-B. Caron. 2015. *Hallucigenia's* head and the pharyngeal armature of early ecdysozoans. *Nature* 523:75.

- Sun, Z., H. Zeng, and F. Zhao. 2020. A new middle Cambrian radiodont from North China: implications for morphological disparity and spatial distribution of hurdiids. *Palaeogeography, Palaeoclimatology, Palaeoecology* 558:109947.
- Tanaka, G., X. Hou, X. Ma, G. D. Edgecombe, and N. J. Strausfeld. 2013. Chelicerate neural ground pattern in a Cambrian great appendage arthropod. *Nature* 502:364–367.
- Waloszek, D., and A. Maas. 2005. The evolutionary history of crustacean segmentation: a fossil-based perspective. *Evolution and Development* 7:515–527.
- Yang, J., J. Ortega-Hernández, H. B. Drage, K.-s. Du, and X.-g. Zhang. 2019. Ecdysis in a stem-group euarthropod from the early Cambrian of China. *Scientific Reports* 9:1–9.
- Yang, X., J. Kimmig, D. Zhai, Y. Liu, S. R. Kimmig, and S. Peng. 2021. A juvenile-rich palaeocommunity of the lower Cambrian Chengjiang biota sheds light on palaeo-boom or palaeo-bust environments. *Nature Ecology and Evolution* 5:1082–1090.
- Zeng, H., F. Zhao, Z. Yin, and M. Zhu. 2018. Morphology of diverse radiodontan head sclerites from the early Cambrian Chengjiang Lagerstätte, south-west China. *Journal of Systematic Palaeontology* 16:1–37.
- Zeng, H., F. C. Zhao, Z. J. Yin, and M. Y. Zhu. 2021. A new early Cambrian bivalved euarthropod from Yunnan, China and general interspecific morphological and size variations in Cambrian hymenocarines. *Palaeoworld* 30:387–397.
- Zhang, X.-L., D.-G. Shu, and D. H. Erwin. 2007. Cambrian naraoiids (Arthropoda): morphology, ontogeny, systematics, and evolutionary relationships. *Paleontological Society Memoir* 81:1–52.